Evolutionary Ecology, 1994, **8**, 369–386

Spatial polymorphism of bacteriocins and other allelopathic traits

STEVEN A. FRANK

Department of Ecology and Evolutionary Biology, University of California, Irvine, CA 92717, USA

Summary

Many bacterial species carry plasmids that encode both the production of a highly specific toxin (bacteriocin) that kills competitors of the same species and immunity to that toxin. A great diversity of bacteriocins is produced within a single species. I present a model for the dynamics of competition between allelopathic and susceptible types. The model applies to most kinds of allelopathic competition. My primary goal is, however, to explain the widespread genetic polymorphism for bacteriocins. The model includes competition for scarce resources, competition through toxin production, spatial diffusion of individuals and toxins at varying rates and spatial variation in habitat quality. I draw three main conclusions from this 'reaction–diffusion' model. (1) Polymorphism of toxin producers and susceptibles cannot be maintained within a single spatial location when individuals and the toxin mix randomly. (2) Susceptibles are generally favoured in poor habitats, where the rate of resource competition per interaction increases relative to the resource-independent rate of toxic killing. By contrast, toxic producers are generally favoured in good habitats, where the rate of resource competition is lower. (3) Spatial variation in habitat quality can lead to spatial polymorphism; susceptibles tend to win in poor habitats and producers tend to win in good habitats.

Keywords: colicin; competition; migration; reaction–diffusion; plasmid

Introduction

Bacteria often carry plasmids that encode both a bacterial toxin (bacteriocin) and immunity to that toxin (Reeves, 1972; Hardy, 1975; Lewin, 1977). Immunity works by neutralizing the toxin after it has entered the cell. Bacteria may also be resistant to bacteriocins because they lack a compatible receptor through which the toxin can enter the cell.

Many distinct bacteriocin types are found within a population. A type is defined by its susceptibility to a set of toxin-producing test strains. With n test strains, there are 2^n possible types. Epidemiological studies frequently use bacteriocin typing to identify and follow pathogenic strains of bacteria. These studies provide information about the diversity of bacteriocin production and susceptibility in populations. For example, Chhibber *et al.* (1988) summarize data on the number of isolates, test strains and bacteriocin susceptibilities for 10 studies of *Klebsiella pneumoniae*. The fewest number of observed types occurred in a study with 200 isolates, four test strains and 11 types of a possible $2^4 = 16$; the most occurred in a study with 553 isolates, seven test strains and 64 types of a possible $2^7 = 128$. Similar levels of diversity have been reported for a variety of species (Gaston *et al.*, 1989; Senior and Vörös, 1989; Rocha and de Uzeda, 1990; Traub, 1991; Riley and Gordon, 1992).

The processes that maintain bacteriocin polymorphism are not understood. Here I develop models for the dynamics of competition between producer and susceptible strains. I assume that producer strains pay a cost for toxin production or plasmid carriage in terms of a relatively lower intrinsic rate of increase, but gain the benefit of killing a fraction of the susceptible competitors at a specified rate.

0269–7653

The models apply generally to many kinds of allelopathy because I make no assumptions that are specific to bacteria. The models are based on the traditional equations for competition between species and can be applied directly to the dynamics of plant communities influenced by allelopathy (Rice, 1984). In order to apply the model to bacteriocins, I assume that plasmids are non-conjugative and therefore transmitted as strain (species)-specific genes.

In the first part of the paper I show that polymorphism within a single spatial location cannot be maintained when individuals and the toxin mix randomly (Adams *et al.*, 1979; Chao and Levin, 1981; Levin, 1988). Initial abundances affect the competition. When producers are common, rare susceptibles typically fail to increase because of the high concentration of toxin in the habitat. When susceptibles are common, rare producers typically fail to increase because the tiny amount of toxin produced has virtually no effect on the resident susceptibles and the susceptibles are superior competitors for scarce resources.

The strength of resource-dependent competition between strains relative to the rate of killing by toxins also plays a key role in determining who wins the competition. When resource competition is intense, susceptibles win because the effects of direct competition overwhelm the effects of toxic killing. When resources are abundant, producers win because toxic killing is the primary competitive interaction.

In the second part of the paper I analyse the effects of migration, spatial diffusion of the toxin and spatial variation in habitat quality on the maintenance of polymorphism. Spatial variation in habitat quality can lead to spatial polymorphism; susceptibles tend to win in poor habitats and producers tend to win in good habitats. The space–time dynamics are interesting because relative abundance also influences the local dynamics, and relative abundance is determined by the initial abundances, competition among neighbouring strains and spatial diffusion of individuals and the toxin.

There is a rich mathematical literature on reaction–diffusion models of Lotka–Volterra dynamics (e.g. Levin, 1979; Mimura, 1984; Mimura *et al.*, 1991). The spatial pattern in the abundances of competing species occurs under a variety of assumptions about diffusion, spatial heterogeneity and the shape of the habitat. The models here differ in detail but do not present any new concepts. Rather, my purpose is to explain some laboratory observations from bacteria and to present clear explanations for the dynamics when there is an interaction between allelopathy and spatial heterogeneity in habitat quality. These preliminary models form the basis on which to build theories that explain the widespread polymorphisms of bacteriocins.

The model

The dynamics of allelopathic and susceptible strains can be modelled by a system with three 'reactants'. The abundances (concentrations) of the producer strain, P, and susceptible strain, S, interact with the abundance of the allelopathic substance, A. The abundances may vary over space, so that local abundances depend on both the reaction determined by the local concentrations and the diffusion of reactants from other locations. The local abundance of each reactant is therefore a function of time, t, and spatial location, $\mathbf{x}$, where $\mathbf{x}$ is a location vector in n dimensions.

The following equations describe this reaction–diffusion system

$$\frac{\partial P}{\partial t} = \gamma P\left[(1-\alpha) - \frac{(1-\alpha)P + S}{K}\right] + D_1\nabla^2 P \tag{1a}$$

$$\frac{\partial S}{\partial t} = \gamma S\left[1 - \frac{(1-\alpha)P + S}{K}\right] - \delta AS + D_1\nabla^2 S \tag{1b}$$

$$\frac{\partial A}{\partial t} = \beta P - \rho A + D_2 \nabla^2 A \tag{1c}$$

Lokta–Volterra assumptions determine growth and resource-dependent competition between strains. The strains have the same maximum rate of increase, γ, but the producers pay a cost given as α, the proportional decrease in maximal growth; α ranges between 0 and 1. The strains compete directly for limited resources. The environment can support K individuals.

Levin's (1988) assumptions specify the production of toxin and the rate of toxic deaths among susceptibles. Toxin molecules are produced at a rate, β, per producer individual and molecules decay at a rate, ρ. Toxic deaths increase linearly with concentration of the toxin, A, and a rate parameter, δ.

Spatial diffusion causes movement of individuals at rate D_1 and toxins at rate D_2. The ∇^2 terms are the vectors of second partial derivatives in concentration in the n spatial dimensions $(\partial^2/\partial x_1^2, \ldots, \partial^2/\partial x_n^2)$. Roughly speaking, the diffusion terms cause a location's concentration of reactants to be averaged over the concentrations of the reactants in the neighbouring locations. This averaging occurs over time at a rate that is set by the diffusion coefficients, D_1 and D_2. (Murray (1989) gives a general introduction to reaction–diffusion models in biology.)

All parameters are positive and all abundances and concentrations are non-negative.

Spatially homogeneous cases

The system in Equations la–lc describes the spatially homogeneous case when concentrations are independent of spatial location and all second partial derivatives in space are zero ($\nabla^2 = 0$ for any reactant P, S or A). This system is easier to analyse when rewritten in non-dimensional form (Segel, 1972; Murray, 1989). Non-dimensional analysis focuses attention on a minimal set of parameters and highlights relative magnitudes (scaling relations) among the processes that drive the dynamics. This is accomplished without altering the dynamics or interpretation because one can translate freely between the biologically motivated formulation and the non-dimensional quantities.

The system in Equations 1a–1c, with $\nabla^2 = 0$, can be rewritten with the following substitutions

$$\begin{aligned} &\hat{P} = P/K, \qquad \hat{S} = S/K, \qquad \hat{A} = A\gamma/\beta K, \\ &\tau = \gamma t, \qquad g = K\delta\beta/\gamma^2, \qquad b = \rho/\gamma \end{aligned} \tag{2}$$

The biological meaning of the new parameters will be discussed later. Dropping the hats yields the non-dimensional, spatially homogeneous system

$$\frac{dP}{d\tau} = P[(1 - \alpha) - (1 - \alpha)P - S] \tag{3a}$$

$$\frac{dS}{d\tau} = S[1 - (1 - \alpha)P - S] - gAS \tag{3b}$$

$$\frac{dA}{d\tau} = P - bA \tag{3c}$$

where the reactants are now functions only of time and, therefore, these are ordinary rather than partial differential equations.

Contact inhibition

Many interesting properties of allelopathy can be seen after one further simplification of Equations 3a–3c. Suppose that toxic killing occurs only when an individual of the P strain physically touches an S individual. The system is now described by replacing the term δAS in Equation 1b with δPS, where δ is the killing rate per contact, and by dropping the equation for the concentration of the toxin, A, because there is no diffusible molecule in this case. I will return to the role of diffusible toxins in the next section.

Using the same non-dimensional substitutions as in Equation 2, with the simplified substitution $g = \delta K/\gamma$, yields the system

$$\frac{dP}{d\tau} = P[(1 - \alpha) - (1 - \alpha)P - S] \tag{4a}$$

$$\frac{dS}{d\tau} = S[1 - (1 - \alpha)P - S] - gPS \tag{4b}$$

This system has two 'reactants', P and S, whose abundances are given by the fractions of the carrying capacity, K. The two parameters are α, which is the cost of the killing mechanism and g, which is the killing rate per contact scaled by the carrying capacity, K, and standardized to the non-dimensional time measure $1/\gamma$. Scaling by K occurs because interaction between individuals has two distinct negative fitness effects: resource competition and contact inhibition. The larger K, the weaker the force of resource competition relative to contact inhibition per interaction.

I analyse the qualitative dynamics of Equation 4 by phase plane methods. Odell (1980) gives an excellent introduction to this technique. The goal is to show the direction of change in P and S for a pair of values for $P(\tau)$ and $S(\tau)$ at time τ.

The first step is to plot the nullclines, that is, where $dP = 0$ or $dS = 0$ so that the system is changing in only one direction (Fig. 1). Solving $dP = 0$ shows that P does not change along either of two nullclines, $P = 0$ or $S = (1 - \alpha)(1 - P)$. Change under these conditions is only in the vertical direction. This is shown with the arrows pointing up along the $P = 0$ axis and the arrows pointing up or down along the other nullcline. The direction of the arrows is determined by the sign of dS when $dP = 0$. Similarly, solving $dS = 0$ shows that S does not change when either $S = 0$ or $S = 1 - (1 - \alpha + g)P$. The directions of the arrows along these two nullclines are determined by the sign of dP when $dS = 0$.

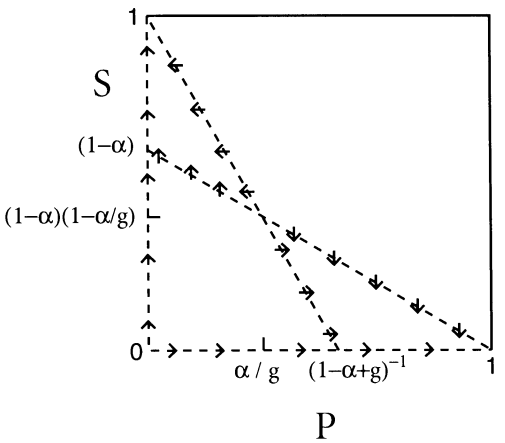

Figure 1. Equilibria and nullclines for the contact inhibition model given by Equations 4a and 4b.

The system is in equilibrium only where the $dP = 0$ and $dS = 0$ nullclines cross. These crossings occur at four locations. If we write ordered pairs (P,S) for locations in Fig. 1, then equilibria occur at (0,0) (0,1) (1,0) and (P^*,S^*). The values of $P^* = \alpha/g$ and $S^* = (1 - \alpha)(1 - \alpha/g)$ give the point at which the two internal nullclines cross.

When $\alpha > g$ the lines do not cross for positive S and P values, and there is no mixed equilibrium with both S and P present. In this case the only stable state for the system is a population of pure susceptible individuals, $S = 1$, with no producers, $P = 0$. For any initial abundance of P, a small number of S individuals can increase their abundance to the carrying capacity and drive P to 0.

The dynamics for $g > \alpha$ are shown in Fig. 2. The system evolves quickly to one of two stable states: a pure population of producers or a pure population of susceptibles. Populations that are initially dominated by producers will evolve to a state of pure producers; populations that are initially dominated by susceptibles will evolve to a state of pure susceptibles. The basins of attraction for the two stable states are shown by the shading in Fig. 2. Initial abundances for producers and susceptibles, $P(0)$ and $S(0)$, that fall in the shaded areas are attracted to the pure producer equilibrium, whereas initial abundances in the unshaded areas are attracted to the pure susceptible equilibrium. Adams *et al.* (1979), Chao and Levin (1981) and Levin (1988) described the disruptive frequency dependence of this system but did not provide analytic solutions.

The 'separatrix' is the curve dividing the basins of attraction given the initial values $P(0)$ and $S(0)$. The separatrix includes the points (0, 0) and the internal equilibrium (P^*, S^*) and is nearly linear when α is not too close to 1. Thus, the internal equilibrium is sufficient to draw a very good approximation for the location of the separatrix and the basins of attraction. When the cost of the killing mechanism, α, increases, the basin of attraction for P shrinks; when the rate of killing per contact increases relative to the strength of resource-dependent competition, $g = \delta K/\gamma$, the basin of attraction for P increases.

Finally, two technical points are useful for comparison with more realistic models developed in the following sections. First, the final outcome – fixation of S or P – depends on four conditions: two initial values, $P(0)$ and $S(0)$, and two non-dimensional parameters, α and g (Fig. 2). Second,

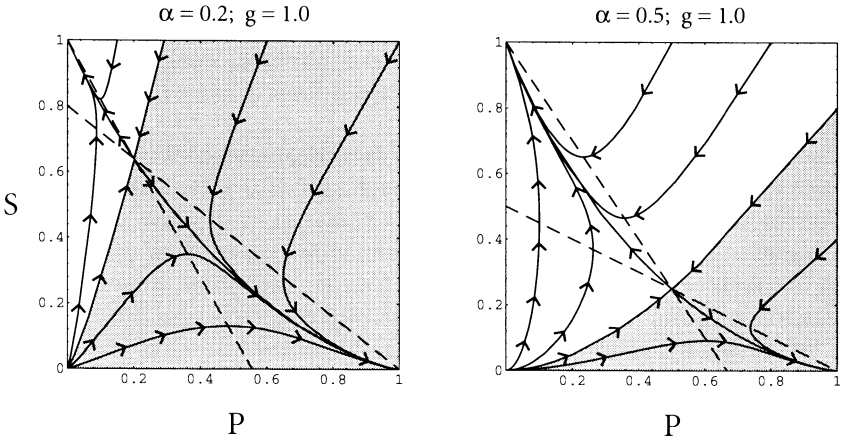

Figure 2. Temporal dynamics for the contact inhibition model given by Equations 4a and 4b. The shaded region shows the basin of attraction for the stable end-point of pure producers. The unshaded region shows the basin of attraction for the stable end-point of pure susceptibles. The curve dividing the basins of attraction is called the 'separatrix', which lies along the stable flow that moves from the origin toward the internal equilibrium.

the internal equilibrium is a 'saddle' because the dynamical flow moves toward the point in one direction and away from the point in another direction (Fig. 2). This can be shown analytically by the fact that the eigenvalues of Equations 4a and 4b are of opposite sign at the internal equilibrium when the internal equilibrium exists ($g > \alpha$). Each positive eigenvalue characterizes flow away from the equilibrium in one dimension, and each negative eigenvalue characterizes flow toward the equilibrium in one dimension.

Diffusible toxin

If the killing mechanism is a diffusible toxin molecule with concentration A, then we return to the system in Equations 3a–3c with P, S and A. The overall pattern of the dynamics is the same as for contact inhibition described in the previous section: when P is initially abundant and S rare, then the system typically stabilizes at the pure P state, whereas when P is initially rare and S abundant, then the system typically stabilizes at the pure S state.

This system is more complex, however, because the initial abundance of the toxin molecule, A, also influences the dynamics. Thus, there are three initial values, $P(0)$, $S(0)$ and $A(0)$. There are also three parameters now: α is the cost of toxin production by the producer strain, $b = \rho/\gamma$ is the decay rate of the toxin on the non-dimensional time scale, $1/\gamma$ and $g = (\delta/\gamma)\,(\beta/\gamma)\,K$ is the product of the killing rate per contact between the molecule and susceptible individual, δ, with the toxin production rate, β, relative to the strength of the resource-dependent competition per interaction, $1/K$. These rates are scaled to the non-dimensional time frame $1/\gamma$.

The system has four equilibria. Given as (P, S, A) triplets, the equilibria are (0, 0, 0), pure susceptibles at (0, 1, 0), pure producers at (1, 0, $1/b$) and a mixed internal equilibrium at (P^*, S^*, A^*). The solution for the mixed equilibrium is $P^* = b\,\alpha/g$, $S^* = (1 - \alpha)\,(1 - P^*)$ and $A^* = P^*/b$. The internal equilibrium does not exist when $b\,\alpha > g$. In this case the system evolves to pure susceptibles when some susceptible individuals are present, $S(0) > 0$.

The internal equilibrium, when it exists, is a saddle point with one positive and two negative eigenvalues. The one-dimensional unstable flow away from the equilibrium goes towards one of the two stable equilibria with either pure producers or pure susceptibles, similar to the arrangement shown in Fig. 2. The two-dimensional stable flow is a surface containing trajectories that move towards the internal equilibrium. As in Fig. 2, one corner of the surface includes the origin. This surface forms the separatrix that divides initial conditions, $P(0)$, $S(0)$ and $A(0)$, into two distinct basins of attraction that lead either to pure susceptibles or pure producers (Adams *et al.*, 1979; Chao and Levin, 1981; Levin, 1988).

The location of the separatrix is shown in Fig. 3 for a 2^3 factorial combination of the parameters α, g, and b. The lower left panel shows the structure of each plot. The initial conditions $P(0)$ and $S(0)$ are given along the axes as labelled. The contours show the projection of the separatrix surface for three different initial concentrations of the toxin, $A(0)$: the contour on the right shows the separatrix when the toxin is absent initially; the contour in the middle shows the separatrix when toxin concentration is in equilibrium with the abundance of producers, $A(0) = P(0/)b$; and the contour on the left shows the separatrix when the initial concentration of the toxin is at its maximum, which occurs when the population is pure producers, $P = 1$. For each contour (initial value of A), initial conditions for P and S to the right lead to fixation of the producers, and to the left lead to fixation of the susceptibles.

The middle contour in each panel of Fig. 3 includes the internal equilibrium point, shown by a filled circle. A rough approximation for the location of the basins of attraction can be made by noting that the separatrix surface contains (0, 0, 0) and has the internal equilibrium near its middle. Because $S^* = (1 - \alpha)\,(1 - P^*)$ and $P^* = b\alpha/g$, the basins of attraction are controlled mainly by P^*. Low values of P^* widen the basin of attraction for the producers, P.

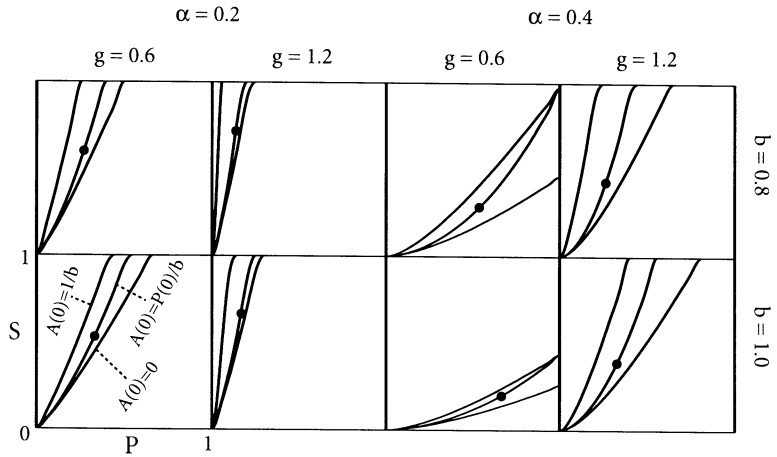

Figure 3. Contour plots for the separatrix in the spatially homogeneous model with diffusible toxins given by Equations 3a–3c.

To summarize, the system evolves to pure producers or pure susceptibles. The particular outcome depends mainly on the initial abundances of the producers and susceptibles, and less strongly on the initial concentration of the toxin. Whether a particular set of initial conditions leads to pure susceptibles or producers depends on three non-dimensional parameter groupings. Low values for the cost of toxin production, α, and the decay rate of the toxin relative to population growth, b, widen the basin of attraction for the producers. A high value of g also widens the basin of attraction for the producers. This non-dimensional parameter is the product of the toxin's killing rate and production rate relative to the strength of resource-dependent competition per interaction, $1/K$.

Of the various parameters, the habitat quality (carrying capacity) K is likely to vary the most over space and time. As just mentioned, the magnitude of K determines the scaling relationship between the strength of the resource-dependent competition and the resource-independent killing rate of allelopathy.

Diffusion in spatially heterogeneous cases

Spatial variation in habitat quality and initial abundance can strongly influence the population dynamics of allelopathy (Chao and Levin, 1981). The role of spatial variation and migration can be studied in a model with a one-dimensional habitat in which individuals and toxins diffuse across space while individuals simultaneously grow and compete in the ways described above. Two conclusions from the previous sections form the basis for understanding complex spatial interactions: (1) habitat quality, K, subsumed in the non-dimensional parameter g, plays a major role in the location of the separatrix between the basins of attraction for susceptibles and producers, and (2) relative abundance of susceptibles and producers determines which basin of attraction the local population falls into.

Contact inhibition

The key features of spatial dynamics can be seen most easily in the simplified model of contact inhibition. In this case there is no diffusible toxin and allelopathy occurs only when a producer

comes very close to a susceptible individual. The system is described by a spatial version of Equations 4a and 4b

$$\frac{\partial P}{\partial \tau} = P[(1 - \alpha) - c(x)\{(1 - \alpha)P + S\}] + \frac{\partial^2 P}{\partial x^2} \tag{5a}$$

$$\frac{\partial S}{\partial \tau} = S[1 - c(x)\{(1 - \alpha)P + S\}] - gPS + \frac{\partial^2 S}{\partial x^2} \tag{5b}$$

The function $c(x) = K/K(x)$ describes the relative habitat quality at spatial location x, where $K(x)$ is the carrying capacity at location x, and the K is the maximum carrying capacity over space. The scalings for P, S, and g are given relative to K as described above.

The single spatial dimension, x, is measured in non-dimensional units $\hat{x} = x(\gamma/D_1)^{1/2}$. As before, the non-dimensional version is used in Equations 5a and 5b, but the hat is dropped for notational simplicity. Notice that the diffusion rate of individuals, D_1, is absorbed into the new spatial scaling. (See Murray (1989) for a discussion of spatial scaling in diffusion models.)

Six factors determine the dynamics of the system. There are two initial conditions for the spatial distributions of P and S. The parameters g and α retain their meanings from the previous model of contact inhibition. In addition, the distribution of relative habitat quality, $c(x)$, must be specified, along with the total length of the habitat, L, measured in non-dimensional spatial units. Given these six factors, the temporal and spatial evolution of the system can be studied by computer. This is a deterministic model, which means that, for particular initial conditions and parameters, each computer run will give the same results. I provide details of the numerical methods in the Appendix.

In the remainder of this section I provide the details of the numerical analysis. The main conclusions from this section are summarized in the Discussion.

Figure 4 shows the temporal and spatial dynamics in four sample runs. Each run begins at the top of a column, with time moving forward as one moves down a column. Space is given by the x-axis of each panel. At each spatial location the height of the solid curve shows the abundance of P, and the height of the dashed curve shows the abundance of S. Habitat quality has three peaks across the spatial domain, shown by the shapes in the bottom row of panels (see Appendix). The highest peak is the maximum of $K(x)$, which is standardized to a value of 1. The y-axis is on a logarithmic scale covering six orders of magnitude. The midpeak is scaled to the outer peaks by the parameter m, which is the relative height of the midpeak on a $\log_{10}$ scale. In this figure the midpeak is always equal to or smaller than the outer peaks, while in other cases the midpeak may be higher. This habitat pattern is used in all computer studies reported below.

At time zero (not shown), the P and S individuals are equally abundant in a small interval in the middle of the entire length of the habitat, with the sum of the abundances of P and S equal to the carrying capacity in that narrow interval. After the first period of time the distributions are shown in the top panel (see the figure legend for time scaling). So far, all growth and competition has been confined to the middle peak. In the top left panel, S enjoys a 5% growth advantage over P, and the middle peak is of relatively low quality at 1% of the height of the outer peaks. S tends to outcompete P in poor quality habitats (low g, see above) and in this case S has, by growth and diffusion, quickly taken over the middle peak.

Moving from left to right across the top row shows the effects of midpeak scaling, m, and the cost of allelopathy, α. The second panel has the same midpeak height, but S enjoys only a 2% growth advantage. In this case the quality of the habitat is sufficiently low that this 2% advantage allows S to dominate the middle peak. In each of the next two panels to the right, habitat quality in the midpeak increases by one order of magnitude. Increasing habitat quality provides a strong advantage to the producers, P.

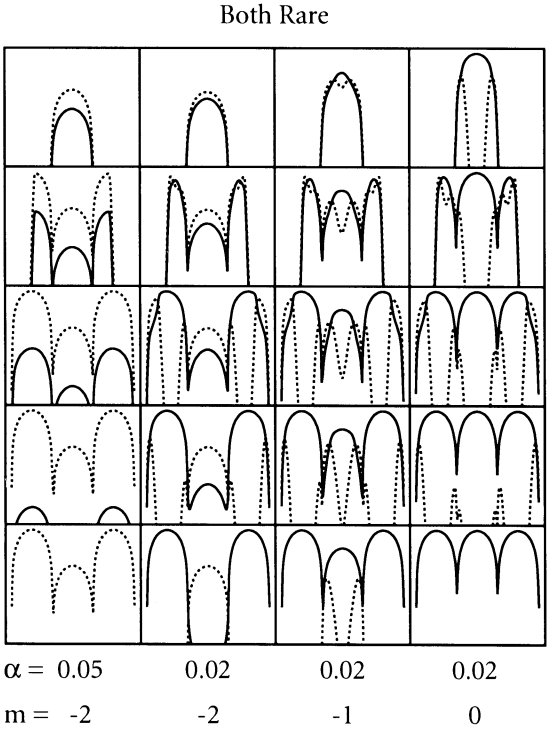

Figure 4. Space–time dynamics for the contact inhibition model in Equations 5a and 5b. Time moves forward from the top row to the bottom row, with non-dimensional times, $\tau = \gamma t$, of 55, 110, 165, 275 and 1000 for the top to bottom rows, respectively. Each column shows a different set of parameters, as labelled at the bottom. Within each panel, the x-axis is the spatial dimension of the habitat. At each spatial location the height of the solid curve shows the abundance of P and the height of the dashed curve shows the abundance of S. Further details are in the text.

Diffusion to the outer peaks is shown in the second row. Initial colonization of the outer peaks depends mainly on growth and diffusion because, when both types are rare, competition has little effect. In the far left panel, S gets a sizeable initial advantage in the outer peaks because of its relatively large advantage in growth. This initial advantage is sufficiently large to allow S to dominate the outer peaks in spite of the high quality of the habitat. In the dynamical language of the previous section, S has a narrow basin of attraction in the outer peaks but, in the far left column, S enjoys a sufficiently great advantage in initial abundance to fall within this narrow attracting region. The other columns show that, when initial abundance in the outer peaks is not strongly in favour of S, that P outcompetes S because of the high quality of the habitat.

The bottom row, second column shows that spatial polymorphism can arise from an initially symmetric distribution of P and S. In this case, diffusion of P from the outer peaks into the middle happens slowly enough that S can maintain the midpeak between two populations of P that are each two orders of magnitude larger in size. If the distance between peaks were much shorter, then the diffusion of P into the midpeak would be high enough to overwhelm S and the entire habitat would be dominated by P.

Figure 5 summarizes the final outcome for a variety of initial abundances and parameter combinations. The lower left panel shows the structure of each plot. The length of the habitat in non-dimensional units is $L = 10 \times 2^z$, where z is given along the x-axis. Eight values of L are

presented, ranging from 10 to 1280. The height of the midpeak relative to the two outer peaks is 10^m, where m is given along the y-axis. There are seven different midpeak scalings.

The plot itself is divided into 56 squares, one for each combination of length and midpeak scaling. Each square is shaded according to the final outcome for that parameter combination, with four types: (1) black for global dominance by S, (2) dark gray for spatial polymorphism, with S dominating the low peaks and P dominating the high peaks, (3) light gray for cases in which S is rare and confined to the poor-quality habitats in the narrow valleys between peaks and (4) white for global dominance by P.

The initial abundances for the bottom row of Fig. 5 are the same as in Fig. 4: S and P are both rare and confined to the same narrow spatial region in the middle of the habitat. In the top row both types are initially common and equally abundant at each spatial location, with the sum of their abundances equal to the local carrying capacity. The parameters α and g are varied across columns of the figure, as shown by the labelling at the top.

One can get a feeling for how different outcomes occur by matching the time series in Fig. 4 with locations in Fig. 5. The left column in Fig. 4 falls in the lower left panel of Fig. 5 at the (x, y) position $(6, -2)$. This square is black because the outcome is global dominance by S. The second column of Fig. 4 falls at the same position, $(6, -2)$, in the panel in the second column, in the bottom row of Fig. 5. This square is dark gray because the outcome is dominance of high peaks by P and low peaks by S. The third and fourth columns of Fig. 4 are at $(6, -1)$ and $(6, 0)$, up one and two squares, respectively, from the square for the second column – the shift is caused by the

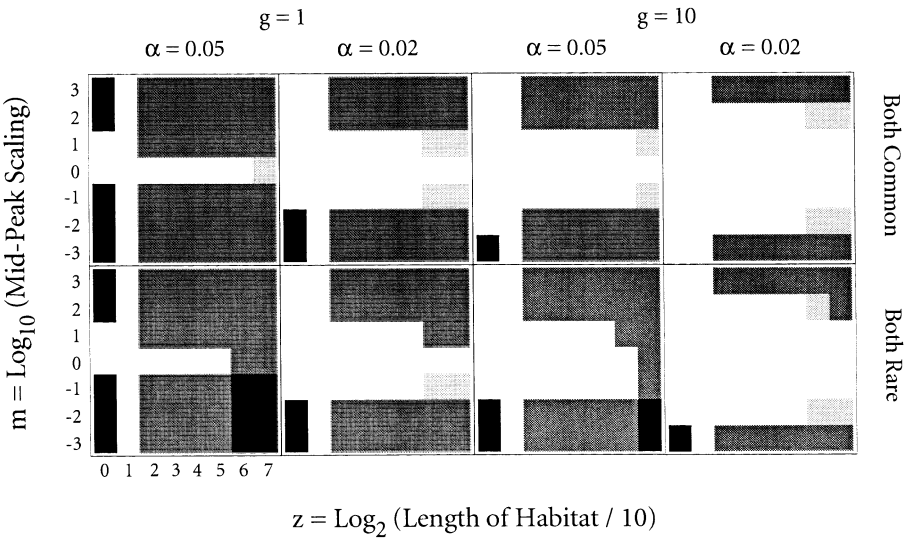

Figure 5. Outcomes of space–time dynamics for symmetric initial distributions of the abundances of P and S. This is a spatially heterogeneous model of contact inhibition. Each panel shows a different parameter combination for g, α and the initial condition. Within each panel the plot is divided into 56 squares, one for each combination of length and midpeak scaling. Each square is shaded according to the final outcome for that parameter combination, with four types: (1) black for global dominance by S, (2) dark gray for spatial polymorphism, with S dominating the low peaks and P dominating the high peaks, (3) light gray for cases in which S is rare and confined to the poor-quality habitats in the narrow valleys between peaks and (4) white for global dominance by P.

increasing value of m. These squares are, respectively, light gray and white, for S confined to valleys and complete dominance by P.

I now draw six conclusions from Fig. 5. The first four are from the top left panel.

(1) S can dominate for small lengths (black stripe for $z = 0, L = 10 \times 2^z$) because the effective habitat quality is low when much of the habitat is near a hostile boundary and individuals often diffuse into uninhabitable regions. If the habitat becomes too short, neither type can survive because death by diffusion off the ends outpaces reproduction (see Okubo, 1980).

(2) P dominates for small lengths ($z = 0$) when the midpeak is an order of magnitude taller than the outer peaks ($m = 1$) but not when the midpeak is an order of magnitude shorter than the outer peaks ($m = -1$). This occurs because the effective habitat quality of the outer peaks is greatly reduced by proximity to the boundaries, whereas the midpeak is not strongly affected. Further, P can outcompete S in the midpeak only when the midpeak is tall and protected by moderately high outer peaks ($m = 0,1$), but not when the outer peaks are low ($m = 2,3$).

(3) P dominates all peak scalings, m, when the length is doubled to $z = 1$. At this length, P wins in two steps. First, P outcompetes S in the highest peak, while S may at first gain an advantage in the lower peaks. Second, because the habitat is relatively short and the peaks are close together, diffusion of P from the high peaks overwhelms the competitive advantage that S enjoys in the low peaks. This shifts relative abundance in the low peaks strongly in favour of P and, thus, allows P to drive S to extinction. Mixed dominance is stable as habitat lengths double again, $z = 2$. In longer habitats the distance between peaks is too great for P to overwhelm S by diffusion from a high peak.

(4) S can survive in valleys between peaks as length becomes much longer. For example, the light gray square appears at the end of the white stripe for $m = 0$ when $z = 7$. Habitat quality is, in general, so poor in the valleys that S can always outcompete P locally, but P may overwhelm S by diffusion into these regions. As the habitat becomes longer, the valleys become wider and diffusion into the valleys declines. At some length S's competitive superiority outweighs the influx of P by diffusion. Thus, many panels show some light gray in the longer habitats.

(5) Moving across panels from left to right, P gains a competitive advantage because the cost of allelopathy, α, declines and the benefit, g, increases. P's advantage is shown by the increase in white area across panels.

(6) Moving from the top to bottom row, S gains an advantage when both types are initially rare rather than initially common. When they are both rare and initially in the midpeak, S has the opportunity to colonize the outer peaks first because of its growth advantage and to maintain dominance because of its initial advantage in relative abundance. This is shown in the left column of Fig. 4. For the same parameters as the left column of Fig. 4, but when both types are initially common, S ultimately dominates the midpeak and P dominates the outer peaks (Fig. 5, upper-left panel, $z = 6$, $m = -2$).

The initial spatial distributions of P and S are identical in Fig. 5. The plots in Fig. 6 have the same parameters and layout, but either P is common and S is very rare (top row) or S is common and P is very rare (bottom row). The methods for these runs are explained in the Appendix. I summarize four conclusions from Fig. 6.

(1) The common type has a large advantage, as discussed above. In particular, the top panels are mostly white because P, when initially common, typically continues to dominate part or all of the habitat. Similarly, the lower panels are mostly dark because S, when initially common, typically continues to dominate part or all of the habitat.

(2) In the top left panel, the outcomes for midpeak scaling of $m = -1$ and lengths $z = 4, 5, 6$

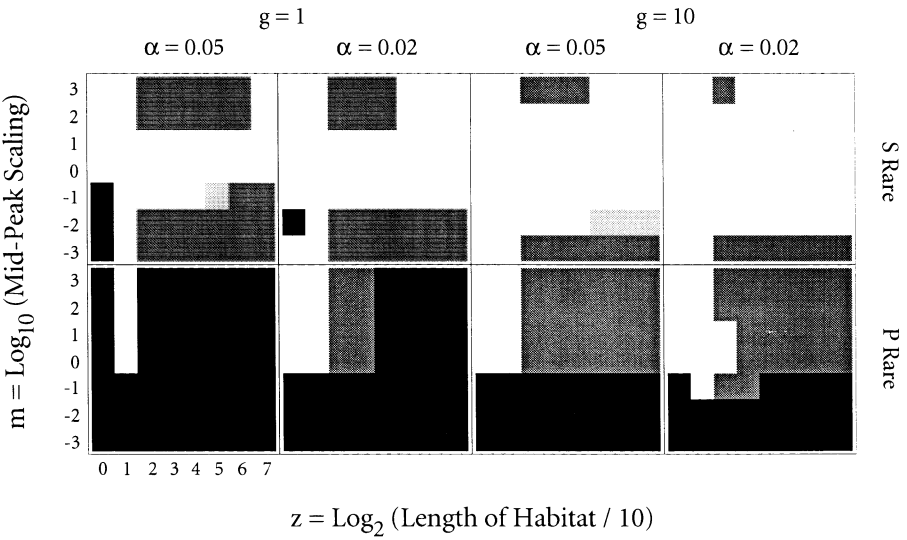

Figure 6. Outcomes of space–time dynamics when one type is initially common and the other type is initially rare. This is a spatially heterogeneous model of contact inhibition.

are, respectively, all P (white), S confined to valleys (light gray) and mixed dominance (dark gray). P apparently wins for the shorter length ($z = 4$) because the invading S individuals diffuse away from the favourably low midpeak and adjacent valleys too rapidly to win in these regions. For the intermediate length ($z = 5$), the balance of S's favourable growth in the valleys and slower diffusion allows the susceptibles to increase in the valleys but, even after a long time ($\tau = 3000$, see Appendix), P still dominates the midpeak. S is apparently held in the valleys because its greater competitive ability in the midpeak is offset by relatively higher losses to diffusion when surrounded by P. For the longer length ($z = 6$), S is able to colonize the midpeak after winning the valleys because of slower diffusion in zones of competition.

(3) The dark gray rectangles in the top part of the upper panels are another example of polymorphism controlled by spatial scaling. In these cases the midpeak is higher than the outer peaks and S, which is initially rare, invades the midpeak. S steadily decreases in the midpeak while diffusing to the outer peaks. When lengths are short, it appears that, in the outer peaks, S's losses to diffusion off the ends of the habitat outpace its growth rate. Thus, P dominates everywhere. At intermediate lengths, S reaches the outer peaks at very low abundance, but then increases steadily because of its competitive advantage in the inferior habitats. Thus, S dominates the outer peaks, whereas P dominates the middle peak. For long lengths, it appears that S's losses from competition in the midpeak are so great that S has been virtually driven to extinction before it reaches the outer peaks. Thus, P dominates the entire habitat for at least the $\tau = 2000$ time-steps studied in this case.

(4) The transitions in the bottom row, second panel from the left show a different space–time pattern of change. In the top part of the panel the midpeak is higher than or equal to the outer peaks, ($m = 0,1,2,3$), and P, which is initially rare, invades the midpeak. For short lengths P wins the midpeak by outcompeting S in this high quality habitat, then takes over the outer peaks by first increasing through diffusion, then dominating by competition. For intermediate lengths P wins the midpeak by outcompeting S, but cannot win the outer peaks because diffusion is less effective across the increased distance between peaks. For long lengths, the initial inoculum of P

must spread over a longer distance within the midpeak; this lowers the effective size of the inoculum for the midpeak region and prevents P from increasing in abundance.

Diffusible toxin

A spatially heterogeneous model with a diffusible toxin is given by

$$\frac{\partial P}{\partial \tau} = P[(1 - \alpha) - c(x)\{(1 - \alpha)P + S\}] + \frac{\partial^2 P}{\partial x^2} \tag{6a}$$

$$\frac{\partial S}{\partial \tau} = S[1 - c(x)\{(1 - \alpha)P + S\}] - gAS + \frac{\partial^2 S}{\partial x^2} \tag{6b}$$

$$\frac{\partial A}{\partial \tau} = P - bA + D\frac{\partial^2 A}{\partial x^2} \tag{6c}$$

which is the non-dimensional version of Equations 1a–1c with spatial variation in habitat quality and $D = D_2/D_1$. The diffusion parameter, D, is the rate of toxin movement relative to the movement of individuals. The parameter b is the decay rate of toxins on the non-dimensional time scale.

The joint effects of b and D are shown in Fig. 7. The figure has, in addition to b and D, the same parameters and initial conditions as the panel in Fig. 6 in the bottom row, second from the left (call this 'panel X'). With a toxin decay rate of $b = 1.0$, the diffusible toxin model has approximately the same outcomes as the contact inhibition model (compare panel X and the left panels of Fig. 7). A decrease in b provides a strong advantage to the producers (compare the left and right panels of Fig. 7).

An increase in the toxin diffusion rate relative to the movement of individuals, D, has two effects. First, when the habitat is short, a high D causes the toxin to diffuse rapidly out of the habitat, thus favouring the susceptibles (compare, for $z = 0$, $D = 1$ versus $D = 10$ in Fig. 7). Second, when the habitat is long, a high value of D increases the chance of successful invasion by the producers (compare, for large L, $D = 1$ versus $D = 10$ in Fig. 7). This is particularly true when rapid diffusion is coupled with a low decay rate (right panel of Fig. 7).

Discussion

Summary of the model

Spatial variation in habitat quality can maintain widespread spatial polymorphism in allelopathy. Seven factors shape patterns of polymorphism in the model.

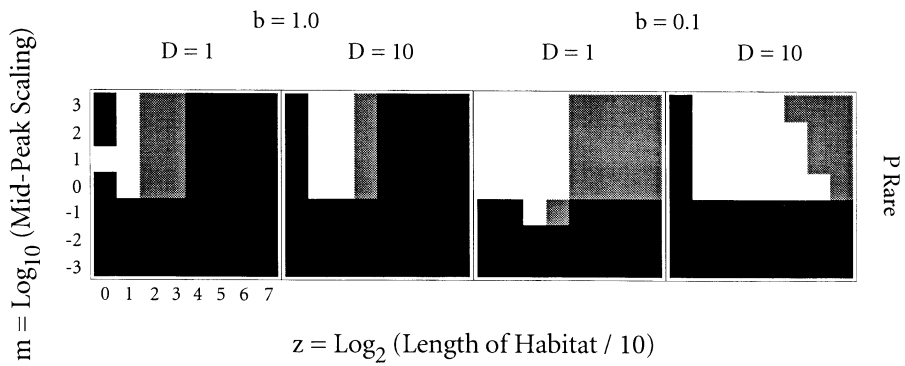

Figure 7. Outcomes of space–time dynamics for a spatially heterogeneous model with diffusible toxin. For these runs $\alpha = 0.02$ and $g = 1$.

(1) Frequency dependence favours whichever type, susceptible or producer, is common (Fig. 2; Adams *et al.*, 1979; Chao and Levin, 1981; Levin, 1988).

(2) The cost of carrying the production-immunity system, α, influences which initial abundances favour pure susceptibles or pure producers (Fig. 2). Small costs are sufficient to maintain widespread polymorphism. For example, I assumed a cost of 2 or 5% in all numerical studies (Figs 4–7).

(3) The relative rate at which resource competition and toxic killing affect growth, g, also influences which initial abundances favour pure susceptibles or pure producers (Fig. 2). This factor is typically more important than α because the rate of resource competition is inversely proportional to habitat quality, K, which often varies over many orders of magnitude.

(4) Spatial variation in habitat quality will cause the favoured type to switch between producers and susceptibles (Fig. 4). High quality habitats favour producers, whereas low quality habitats favour susceptibles. Figures 5–7 show the spatial patterns of polymorphism that result from habitat heterogeneity. This type of spatial variation is similar to Grime's (1977) tolerance–intolerance gradient, in which intolerant species dominate in rich habitats, like producers, and tolerant species dominate in poor habitats, like susceptibles (see also Rosenzweig, 1987, 1991).

(5) The migration (diffusion) rate of individuals, D_1, affects colonization of new habitats and, thus, initial abundances. Migration also influences the relative strength of competitive advantage versus immigration that determines which type wins in a particular location (see Figs 5–7, in which D_1 is subsumed in L).

(6) The diffusion of toxins, D_2, has two opposing effects on the success of the producers. A relatively high diffusion rate may enhance the producers' colonization of neighbouring habitats by reducing the abundance of competitors in advance of a wave of immigration. If the habitat is too short, however, the toxin diffuses rapidly and never builds to a high concentration in any location, thus the producers' competitive ability is reduced (Fig. 7).

(7) The success of the producers increases as the decay rate of toxins, b, declines (Fig. 7).

Limitations of the model in explaining bacteriocin polymorphism

The results of the model apply to any simple system of allelopathy in which susceptible and producer strains compete. Several aspects of bacteriocin polymorphism were not addressed.

(1) The model assumed only one allelopathic type, whereas a great diversity of bacteriocin types occurs within each bacterial species (see the Introduction). Multiple types can influence the conditions for the maintenance of polymorphism, but the details will depend on the patterns of susceptibility and toxicity for each genetic variant. In models for two other co-evolutionary systems, an increase in the number of possible genotypes reduced the need for pleiotropic costs (α) to maintain widespread polymorphism (Frank, 1989, 1993).

(2) The model did not address the distinction between immunity and resistance to bacteriocins. Immunity works by neutralizing the toxin after it has entered the cell. Resistance occurs when a bacterium lacks a compatible receptor through which the bacteriocin can enter the cell. These surface receptors, which are probably used for the uptake of important nutrients, may also be a point of entry by bacteriophages (Hardy, 1975). A complete analysis of bacteriocin polymorphism must explain the distributions of production, immunity and resistance while accounting for the role of receptors in resource acquisition and resistance to bacteriophages.

(3) Toxin decay and diffusion rates may vary spatially. For example, some authors have suggested that bacteriocin toxins, which are proteins, cannot survive long in mammalian stomachs (review in Hardy, 1975).

(4) Genes coding for toxin production and immunity may be transmitted horizontally. This

clearly occurs for many bacteriocins, which are carried on conjugative plasmids. Some bacteriocins are, however, on small non-conjugative plasmids. Horizontal transfer may occur in other allelopathic systems. For example, allelochemicals in plants may sometimes be produced by fungal or bacterial root symbionts.

(5) On the ecological side, I have not explicitly modelled resources used by the bacteria, but rather I have described resource competition and habitat quality in terms of the carrying capacity, N. The type of extension that would be needed to model resources explicitly can be found in Levin (1988).

Other allelopathic systems

I have focused on bacteriocins, although the model applies to polymorphism in any allelopathic system. In fact, the model is based on the traditional equations for between-species interactions and applies directly to competition between producer and susceptible species.

There is a large amount of literature on allelopathy in plants (Rice, 1984) and marine organisms (Thompson, 1985; Thompson *et al.*, 1985), but there are no reports of within-species polymorphism for intraspecific toxicity and immunity. Allelopathic research has, for economic reasons, focused on interference between species. Interference within species is much more difficult to observe than strong between-species interactions. It seems inevitable that, in at least a few cases, genetic polymorphism for toxicity and immunity occurs. The interesting question is whether such polymorphism is common or rare.

Cytoplasmic symbionts occur in *Paramecium* and yeast that have intraspecific allelopathic properties similar to bacteriocins (Grun, 1976). These killer particles are widely distributed in natural populations. Many genetic and biochemical details of killer particles have been analysed in the laboratory, but little is known about their population dynamics and polymorphism under natural conditions. The particular details of transmission and toxicity differ among killer particles, bacteriocin plasmids and plant and marine allelopathy, but all these systems affect competition and the distribution of variety in natural communities.

Acknowledgements

I thank R. M. Bush and B. R. Levin for helpful comments on the manuscript. This research is supported by NSF grant BSR-9057331 and NIH grants GM42403 and BRSG-S07-RR07008.

References

Adams, J., Kinney, T., Thompson, S., Rubin, L. and Helling, R.B. (1979) Frequency-dependent selection for plasmid-containing cells of *E. coli*. *Genetics* **91**, 627–37.

Ames, W. F. 1992. *Numerical Methods for Partial Differential Equations*, 3rd edn. Academic Press, New York.

Chao, L. and Levin, B.R. (1981) Structured habitats and the evolution of anticompetitor toxins in bacteria. *Proc. Natl Acad. Sci. USA* **78**, 6324–8.

Chhibber, S., Goel, A., Kapoor, N., Saxena, M. and Vadehra, D.V. (1988) Bacteriocin (klebocin) typing of clinical isolates of *Klebsiella pneumoniae*. *Eur. J. Epidemiol.* **4**, 115–18.

Fisher, R.A. (1937) The wave of advance of advantageous genes. *Ann. Eugen.* **7**, 355–69.

Frank, S.A. (1989) The evolutionary dynamics of cytoplasmic male sterility. *Am. Nat.* **133**, 345–76.

Frank, S.A. (1993) Coevolutionary genetics of plants and pathogens. *Evol. Ecol.* **7**, 45–75.

Gaston, M.A., Strickland, M.A., Ayling-Smith, B.A. and Pitt, T.L. (1989) Epidemiological typing of *Enterobacter aerogenes*. *J. Clin. Microbiol.* **27**, 564–5.

Grime, J.P. (1977) Evidence for the existence of three primary strategies in plants and its relevance to ecological and evolutionary theory. *Am. Nat.* **111**, 1169–94.
Grun, P. (1976) *Cytoplasmic Genetics and Evolution*. Columbia University Press, New York.
Hardy, K.G. (1975) Colicinogeny and related phenomena. *Bacteriol. Rev.* **39**, 464–515.
Levin, B.R. (1988) Frequency-dependent selection in bacterial populations. *Phil. Trans. R. Soc. Lond. B* **319**, 459–72.
Levin, S.A. (1979) Non-uniform stable solutions to reaction–diffusion equations: applications to ecological pattern formation. In *Pattern formation by dynamic systems and pattern recognition* (H. Haken, ed.), pp. 210–22. Springer-Verlag, New York.
Lewin, B. (1977) *Gene Expression, Volume 3: Plasmids and Phages*. Wiley, New York.
Mimura, M. (1984) Spatial distribution of competing species. In *Mathematical ecology. Lecture notes in biomathematics* Vol. 54 (S. A. Levin and T. G. Hallam, eds), pp. 492–501. Springer-Verlag, New York.
Mimura, M., Ei, S.-I. and Fang, Q. (1991) Effect of domain-shape on coexistence problems in a competition-diffusion system. *J. Math. Biol.* **29**, 219–37.
Murray, J.D. (1989) *Mathematical Biology*. Springer-Verlag, New York.
Odell, G.M. (1980) Qualitative theory of systems of ordinary differential equations, including phase plane analysis and the use of the Hopf bifurcation theorem. In *Mathematical models in molecular and cellular biology*. (L.A. Segel, ed.), pp. 649–727. Cambridge University Press, Cambridge.
Okubo, A. (1980) *Diffusion and Ecological Problems: Mathematical Models*. Springer-Verlag, New York.
Press, W.H., Teukolsky, S.A., Vetterling, W.T. and Flannery, B.P. (1992) *Numerical Recipes in C*, 2nd edn. Cambridge University Press, Cambridge.
Reeves, P. (1972) *The Bacteriocins*. Springer-Verlag, New York.
Rice, E.L. (1984) *Allelopathy*. Academic Press, New York.
Riley, M.A. and Gordon, D.M. (1992) A survey of Col plasmids in natural isolates of *Escherichia coli* and an investigation into the stability of Col-plasmid lineages. *J. Gen. Microbiol.* **138**, 1345–52.
Rocha, E.R. and de Uzeda, M. (1990) Antagonism among *Bacteriodes fragilis* group strains isolated from middle ear exudates from patients with chronic suppurative otitis media. *Ear, Nose, Throat J.*, **69**, 614–18.
Rosenzweig, M.L. (1987) Community organization from the point of view of habitat selectors. In *Organization of communities: past and present* (J.H.R. Gee and P.S. Giller, eds), pp. 469–90. Blackwell Scientific, Oxford.
Rosenzweig, M.L. (1991) Habitat selection and population interactions: the search for mechanism. *Am. Nat.* **137**, S5–S28.
Segel, L.A. (1972) Simplification and scaling. *SIAM Rev.*, **14**, 547–71.
Senior, B.W. and Vörös, S. (1989) Discovery of new morganocin types of *Morganella morganii* in strains of diverse serotype and the apparent independence of bacteriocin type from serotype of strains. *J. Med. Microbiol.* **29**, 89–93.
Thompson, J.E. (1985) Exudation of biologically-active metabolites in the sponge *Aplysina fistularis*. I. Biological evidence. *Marine Biol.* **88**, 23–6.
Thompson, J.E., Walker, R.P. and Faulkner, D.J. (1985) Screening and bioassays for biologically-active substances from forty marine sponge species from San Diego, California. *Marine Biol.* **88**, 11–21.
Traub, W.H. (1991) Bacteriocin typing and biotyping of clinical isolates of *Serratia marcescens*. *Int. J. Med. Microbiol.* **275**, 474–86.
Twizell, E.H., Wang, Y. and Price, W.G. (1990) Chaos-free numerical solutions of reaction – diffusion equations. *Proc. R. Soc. Lond. A* **430**, 541–76.

Appendix

PDE numerical methods and the space–time grid

Numerical techniques for partial differential equations (PDEs) must be chosen according to the specific form of the equations (Ames, 1992). By contrast with ordinary differential equations or

root-finding problems, which can often be solved by standard algorithms (Press *et al.*, 1992), a PDE system may require some modification of existing methods to fit the problem at hand. PDEs are also more difficult because of the computational burden of analysing dynamics in both space and time. Algorithms must therefore be computationally efficient as well as accurate.

To study Equations 5 and 6, I extended the method used by Twizell *et al.* (1990) for the Fisher (1937) equation, which is the classic growth and diffusion model for logistic (Lotka–Volterra) dynamics of a single population. In particular, my extensions allow computationally efficient study of reaction–diffusion models for Lotka–Volterra community dynamics. I briefly outline my method. See Press *et al.* (1992) and Ames (1992) for general background material and definitions of PDE jargon and Twizell *et al.* (1990) for more on the particular approach taken here.

The method uses the Crank–Nicolson scheme for spatial diffusion and a mixture of explicit and implicit difference terms for the reaction (growth, competition and allelopathy). The finite difference equations for the contact inhibition model in Equations 5a and 5b are

$$\begin{aligned} P_i' - P_i = {} & kP_i[a - c(i)(aP_i')] - kc(i)S_iP_i' \\ & + \lambda(1-\theta)P_{i+1} - 2\lambda(1-\theta)P_i + \lambda(1-\theta)P_{i-1} \\ & + \lambda\theta P_{i+1}' - 2\lambda\theta P_i' + \lambda\theta P_{i-1}' \\ S_i' - S_i = {} & kS_i[1 - c(i)S_i'] - kS_i'P_i[g + c(i)a] \\ & + \lambda(1-\theta)S_{i+1} - 2\lambda(1-\theta)S_i + \lambda(1-\theta)S_{i-1} \\ & + \lambda\theta S_{i+1}' - 2\lambda\theta S_i' + \lambda\theta S_{i-1}' \end{aligned}$$

where $a = 1 - \alpha$ and primes denote the unknown abundances in the next time step that must be solved for. The parameter θ determines the mixture between explicit (unprimed) and implicit (primed) values used to calculate the effects of spatial diffusion. I used the standard value of $\theta = 1/2$, which is the Crank–Nicolson scheme. The spatial grid points i occur along a single dimension, where each non-dimensional spatial unit is divided into n_x intervals and thus $i = 0,1, \ldots, N$, where $N = n_xL$. The boundaries are hostile, so that $P_i = S_i = 0$ for $i = 0, N$. The finite difference for the non-dimensional time step is $k = \triangle\tau$. Spatial grid length is subsumed in $\lambda = k/h^2$, where $h = \triangle x = 1/n_{xx}$ is the non-dimensional grid length. I used $\triangle\tau = 0.1$ and $\triangle x = 1/3$ for all runs.

The mixture of implicit and explicit values in the reaction terms are chosen to increase stability (Twizell *et al.*, 1990) and to prevent the negative abundances that occur frequently in purely explicit schemes. In addition, this system can be put in a form that can be solved by efficient computational methods. The equation for P can be written as

$$\begin{aligned} & -\lambda\theta P_{i+1}' + [1 + 2\lambda\theta + kc(i)(aP_i + S_i)]P_i' - \lambda\theta P_{i-1}' \\ & \quad = \lambda(1-\theta)P_{i+1} + [1 - 2\lambda(1-\theta) + ka]P_i + \lambda(1-\theta)P_{i-1} \end{aligned}$$

A similar equation can be written for S. The linear system is tridiagonal and can be solved with $O(N)$ calculations, allowing the study of large grids (Press *et al.*, 1992).

In the model for diffusible toxins, the term $kS_i'P_ig$ in the difference approximation for S is replaced by $kS_i'A_ig$ and the following difference approximation for A is used

$$\begin{aligned} A_i' - A_i = {} & k(P_i - bA_i') \\ & + \sigma(1-\theta)A_{i+1} - 2\sigma(1-\theta)A_i + \sigma(1-\theta)A_{i-1} \\ & + \sigma\theta A_{i+1}' - 2\sigma\theta A_i' + \sigma\theta A_{i-1}' \end{aligned}$$

where $\sigma = D\lambda$.

Habitat quality and method for invasions

Habitat quality is given by a series of sine waves

$$K(x) = \epsilon + \frac{1-\epsilon}{2}\left[1 + \sin\left(\frac{-\pi}{2} + \frac{2\pi x\rho}{L}\right)\right]$$

where ϵ is the minimum value of $K(x)$ and ρ is the number of peaks. The notation used above is related by $c(x) = 1/K(x)$ and $i = xn_x$.

I used three peaks ($\rho = 3$) for all runs. The peaks were scaled according to the parameter m. For $m < 0$, the middle peak, which corresponds to the middle $1/\rho$ of the habitat, was scaled by 10^m. For $m > 0$, the outer peaks were scaled by 10^{-m}.

A rare type was introduced to a habitat by changing the abundance at only one grid point, which may be thought of as covering $\triangle x$ of the habitat. When both types were rare and introduced at the same point, then the sum of their abundances was the carrying capacity at that point. When a type invaded an empty habitat or a habitat in which the other type was common, the abundance of the invading type at that grid point was set to the carrying capacity for that point. In the diffusible toxin model, A is initially absent when P is rare and $A_i = P_i/b$ when P is initially common.

Stopping time for assignment of final outcome

Figures 5–7 show parameters for which spatial polymorphism occurs. The state of the system was determined after some finite (non-dimensional) time T of evolution. The state of the system at T may differ from the asymptotic state as $T \to \infty$. For example, S may be initially rare and declining in the midpeak region and absent in the outer peaks. As S declines within the midpeak it also diffuses to the outer peaks. S may arrive at the outer peaks at a very low abundance and only after a very long time, but may be competitively superior in these outer peaks if they are of relatively low quality. Thus, at some large T, the system may shift from essentially fixed for P to a mixed system with S dominating the outer peaks and P dominating the midpeak.

The shifting of states at large T poses two types of problem for analysis. First, very long times, T, are impractical because of limited computational resources. Second, it is difficult to interpret such shifts. For example, suppose that the abundance of S when it arrives at the outer peaks is 20 or more orders of magnitude smaller than P at each grid point. It may in some cases be more realistic to consider such small magnitudes equivalent to local extinction. To create Figs 5–7, I first did runs for all parameter combinations and initial conditions with a final time of $T = 200$ or $T = 1000$. I then re-examined most of the runs with $1000 \leqslant T \leqslant 3000$. The patterns for a given T and the changes as T increased made the trends fairly clear. However, these problems mean that any individual outcome (square) on the transition between different polymorphic classifications may not be accurate asymptotically. Nonetheless, the overall trends are very clear and the accuracy for individual cases is within the bounds set by difficulties of interpreting widely varying scales in abundance.